Majorana Braiding Dynamics on Nanowires

Cássio Sozinho Amorim, Kazuto Ebihara, Ai Yamakage, Yukio Tanaka, and Masatoshi Sato*
Department of Applied Physics, Nagoya University, Nagoya 464-8603, Japan
(Dated: May 21, 2014)

Superconductors hosting long-sought excitations called Majorana fermions may be ultimately used as qubits of fault-tolerant topological quantum computers. A crucial challenge toward the topological quantum computer is to implement quantum operation of nearly degenerate quantum states as a dynamical process of Majorana fermions. In this paper, we investigate the braiding dynamics of Majorana fermions on superconducting nanowires. In a finite size system, a non-adiabatic dynamical process dominates the non-Abelian braiding that operates qubits of Majorana fermions. Our simulations clarify how qubits behave in the real-time braiding process, and elucidate the optimum condition of superconducting nanowires for efficient topological quantum operation.

PACS numbers:

arXiv:1405.5153v1 [cond-mat.mes-hall] 20 May 2014

Introduction— Recent discovery of topological matters provides a novel platform of quantum devices. In particular , topological superconductors naturally realize yet-to-be discovered excitations called Majorana fermions as a collective mode in condensed matter physics [1–3]. Because of the self-antiparticle nature, the isolated Majorana zero modes display unusual physical properties such as non-Abelian anyon statistics, which is of extreme interest in realization of topological quantum computer in reality.

Topological superconductivity was originally recognized in p-wave spin-triplet superconductors [4–7], however, advance on our understanding of topological matters enables us to design it even in a conventional s-wave superconducting state [8–11]. A recent proposed scheme to realize Majorana fermions by using the spin-orbit interaction and Zeeman field [10–14] was eventually applied to a one-dimensional nanowire with proximity induced s-wave pairing [15, 16], which can be fabricated by the present experimental technique [17–22]. Furthermore, varieties of proposals exist in order to improve the experimental accessibility and controllability of Majorana modes [23–35].

In topological quantum computation, quantum operations of qubits are implemented as an exchange process of Majorana zero modes. Thus, a crucial next step toward topological quantum computer is to understand such an operation of collective excitations as a time-dependent dynamical process.

In this paper, we investigate the braiding dynamics of Majorana zero modes on superconducting nanowires. Generalizing proposed methods of Majorana braiding [36–50], we consider a simpler cruciform junction of topologically non-trivial superconducting nanowires. This simple system functions as a quantum NOT gate of a Majorana qubit by switching gates connecting the wires to the cross point. Using this model, we simulate the Majorana braiding by solving the time-dependent Bogoliubov de Genne equation for the nanowires. A non-adiabatic dynamical process dominates the non-Abelian braiding that operates qubits of Majorana fermions. Our simulations clarify how qubits behave in the real-time braiding process, and elucidate the optimum condition of superconducting nanowires for efficient topological quantum operation.

Majorana Braiding— In the low energy limit, one-dimensional topological superconductors reduce to a one-dimensional spinless p_x-wave superconductor. We adopt the spinless p_x-wave superconductor as a model to analyze universal aspects of Majorana dynamics on nanowires,

$$\mathcal{H} = -\mu \sum_{x=1}^{N} c_x^\dagger c_x - \sum_{x=1}^{N-1} \left(\lambda c_x^\dagger c_{x+1} + \Delta e^{i\theta} c_x c_{x+1} + \text{h.c.} \right), \tag{1}$$

where c_x is a spinless fermion operator and μ, λ and $\Delta e^{i\theta}$ are the chemical potential, the hopping integral, and the p-wave pairing potential, respectively. ($\lambda > 0$, $\Delta > 0$.) There are two different topological phases in the spinless p_x-wave superconductor [6]. When $|\mu| < \lambda$, the p_x-wave superconductor realizes a topologically non-trivial superconducting state, and thus it supports a Majorana fermion on each end. In contrast, when $|\mu| > \lambda$, it becomes a topologically trivial state without Majorana end modes. Below, we consider p_x-wave superconducting nanowires in the topologically non-trivial phase.

To braid the Majorana end states, we consider a cruciform junction illustrated in Fig.1 (a), where four topologically non-trivial nanowires (wire 1, 2, 3 and 4) are connected by four gates (gate 1, 2, 3 and 4). The hopping integral λ and the paring potential Δ at the gates are tunable, so one can connect (disconnect) the wires by turning on (off) these parameters at the gates.

Now let us illustrate how one can exchange the Majorana end modes by switching these gates of the cruciform junction. Initially, we prepare the configuration of Fig.2(a), where wires 2 and 4 are connected by turning on gates 2 and 4, while wires 1 and 3 are disconnected. There are six Majorana end states in the initial configuration since two Majorna end states at the inner edge of

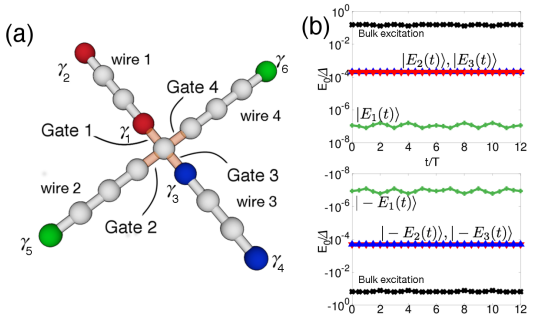

FIG. 1: (color online). (a) Cross-shaped topological superconducting nanowire. The orange junctions connecting to the central site are cut/linked through gate potentials, effectively leaving 4 independently controlled wires. When gates 2 and 4 are connected, while 1 and 3 are shut, six Majorana end modes γ_i $(i = 1, 2, 3, 4, 5, 6)$ are obtained. (b) A typical energy spectrum of MBSs as a function of t, where the time-dependence is given by the gating process in Fig.2. Here we take $\Delta = \lambda$, $\mu = 0.7\lambda$ and $N = 20$. The color of the lines match the color of the modes in Fig.1(a). The finite coupling of MBS on the same wire slightly lifts the zero-mode degeneracy.

wires 2 and 4 are gapped by the coupling at gates 2 and 4.

Counterclockwise exchange of the Majorana modes γ_1 and γ_3, which are localized at the inner edges of wires 1 and 3, can be implemented as follows: First, by turning on the gate 1 [Fig. 2(b)] and then turning off gate 2 [Fig. 2(c)], γ_1 moves to the inner edge of wire 2. Next, γ_3 moves to the inner edge of wire 1 by turning on gate 3 [Fig. 2(d)] and then turning off gate 1 [Fig. 2(e)]. Finally, γ_1 moves to the inner edge of wire 3 by turning on gate 2 [Fig. 2(f)] and then turning off gate 3 [Fig. 2(g)]. The final gate configuration is identical to the initial one, but γ_1 and γ_3 are exchanged.

In the initial configuration $(t = 0)$, wire 1 and wire 3 are isolated from others. While wires 2 and 4 are connected to each other, they are also disconnected from the rest. Due to the finite length of wires, the mixing of Majorana modes occurs between γ_1 and γ_2, γ_3 and γ_4, and γ_5 and γ_6, respectively [6, 51–54]. It induces the following effective coupling between zero modes,

$$\mathcal{H}_{\text{eff}} = i\epsilon\gamma_1\gamma_2 + i\epsilon\gamma_3\gamma_4 + i\epsilon'\gamma_5\gamma_6, \tag{2}$$

where the constants ϵ and ϵ' are real because $\mathcal{H}$ should be hermitian, and ϵ is larger than ϵ' since the coupling between γ_5 and γ_6 is weaker than the others. Assuming the standard anti-commutation relation of Majorana zero modes, *i.e.* $\{\gamma_i, \gamma_j\} = 2\delta_{ij}$, $\mathcal{H}$ can be recast into

$$\mathcal{H}_{\text{eff}} = \epsilon'\left(2c_1^\dagger c_1 - 1\right) + \epsilon\left(2c_2^\dagger c_2 + 2c_3^\dagger c_3 - 2\right) \tag{3}$$

with the Dirac operators

$$c_1 = \frac{\gamma_5 + i\gamma_6}{2}, \quad c_2 = \frac{\gamma_3 + i\gamma_4}{2}, \quad c_3 = \frac{\gamma_1 + i\gamma_2}{2}, \tag{4}$$

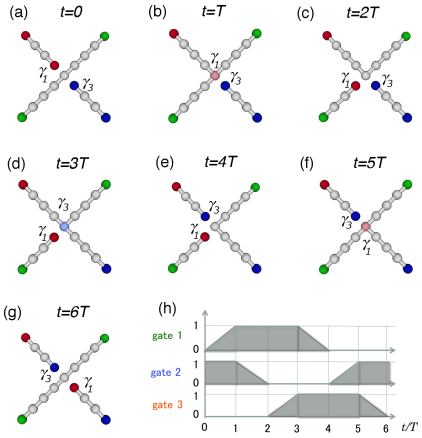

FIG. 2: (color online). The initial conditions of our system is shown in (a), which is operated according to dimensionless gate parameters shown in (h), being 0 a completely separated wire, and 1 a fully connected condition. T is our gate operation time parameter. Majorana γ_1 is moved towards the center in (b) by connecting gate 1 and then to wire 2 in (c) by disconnecting gate 2. Majorana γ_3 is moved from wire 3 to 1 by a similar process in (d) and (e), later taking γ_1 from wire 2 to 3, obtaining an interchange of γ_1 and γ_3.

obeying $\{c_i, c_j^\dagger\} = \delta_{ij}$. Therefore, the mixing results in three negative energy states $|-E_i\rangle$ $(i = 1, 2, 3)$ that are annihilated by c_i,

$$c_i|-E_i\rangle = 0 \tag{5}$$

and three positve partners $|E_i\rangle$ that are annihilated by $c_i^\dagger$,

$$c_i^\dagger|E_i\rangle = 0, \tag{6}$$

with $E_1 = \epsilon'$ and $E_2 = E_3 = \epsilon$.

By switching the gates as described above, we can exchange the Majorana zero modes γ_1 and γ_3. A proper gating process for the non-Abelian braiding does not merely interchange γ_1 and γ_3, but also provide a nontrivial relative phase between them, $\gamma_1 \to -\gamma_3$, $\gamma_3 \to \gamma_1$, or $\gamma_1 \to \gamma_3$, $\gamma_3 \to -\gamma_1$. In both cases, if we exchange γ_1 and γ_3 twice, γ_1 and γ_3 do not go back to the original, but they acquire the minus sign, $\gamma_1 \to -\gamma_1$, $\gamma_3 \to -\gamma_3$. Therefore, after exchange γ_1 and γ_3 twice, the Dirac operators c_2 and c_3 transform into their conjugates $-c_2^\dagger$ and $-c_3^\dagger$ as

$$\begin{aligned} c_2 &= \frac{\gamma_3 + i\gamma_4}{2} \to \frac{-\gamma_3 + i\gamma_4}{2} = -c_2^\dagger. \\ c_3 &= \frac{\gamma_1 + i\gamma_2}{2} \to \frac{-\gamma_1 + i\gamma_2}{2} = -c_3^\dagger, \end{aligned} \tag{7}$$

The nontrivial transformation of c_2 and c_3 implies that the negative energy states $|-E_2\rangle$ and $|-E_3\rangle$, which are annihilated by c_2 and c_3, respectively, end up as the positive energy partners $|E_2\rangle$ and $|E_3\rangle$, and vice versa, after

the exchange process. In other words, if we choose these negative energy states as an initial state, the final state is orthogonal to the initial one. This complete interference is a direct signal of the non-Abelian anyon statistics: Indeed if the system obeys an ordinary Abelian statistics, any exchange process results in a phase factor for any initial state, so the final state cannot be orthogonal to the initial one. The above exchange process defines a quantum NOT gate for Majorana qubits $(|E_2\rangle, |-E_2\rangle)$ and $(|E_3\rangle, |-E_3\rangle)$.

Whereas the above procedure eventually works well as is shown below, the actual implementation needs a careful consideration for the gating. In Fig.1 (b), we show lower energy eigenvalues of the system as a function of t. The eigen energies $E_1(t)$, $E_2(t)$, $E_3(t)$ and their negative energy partners correspond to six Majorana zero modes of the system, where $E_2(t)$ and $E_3(t)$ are degenerate within numerical accuracy as well as their negative energy partners are. At $t = 0$, these eigen energies coincide with E_i $(i = 1, 2, 3)$ in the above, $E_i(0) = E_i$, and we also have $E_i(6T) = E_i(12T) = E_i$ since the system goes back to the initial configuration at $t = 6T$ and $12T$. We note here that there is no level crossing in the energy spectrum in Fig.1 (b), as expected from the von Neumann-Wigner theorem [55]. Therefore, a non-adiabatic transition is needed to achieve the non-Abelian braiding discussed in the above, since any state cannot be different from the original under an adiabatic process. Namely, the gating process in Fig.2 should not be too slow. The non-adiabatic transition is not a classical Landau-Zener transition, because the level spacing rarely depends on t and there is no level approaching to each other at a particular time. We can also argue that a proper gating process should not be too fast at the same time. A fast gating process may create bulk excitations on nanowires, which may give rise to problematic decoherence of Majorana qubits. Therefore, the gating process for non-Abelian braiding should be performed at a proper range of speed.

Below we operate the gates 1, 2, 3 in accordance with the time-sequence diagram in Fig.2 (h). The gating speed can be controlled by an adiabatic parameter T: The gate operation becomes slower (faster) and more adiabatic (non-adiabatic) for larger (smaller) T. A moderate T is required to realize the non-Abelian braiding.

Braiding Dynamics— We now numerically simulate the Majorana braiding process in Fig.2. To numerically evaluate our system, we take each wire length to be the same with one central site linking them. Each gate is represented as a factor $g_i \in [0, 1]$ $(i = 1, 2, 3, 4)$ multiplying the link on the gates in real space [60]. The dynamics of the system is described by the time-dependent Bogoliubov-de Genne equation

$$i\hbar\frac{\partial}{\partial t}\Psi(t) = \mathcal{H}(t)\Psi(t), \tag{8}$$

where $\Psi(t)$ is the quasiparticle wavefunction in the Nambu representation. The evaluation of the wavefunction during a time Δt is given by $\Psi(t + \Delta t) = \mathcal{U}(t + \Delta t; t)\Psi(t)$ with the time-evolution operator $\mathcal{U}(t + \Delta t; t)$,

$$\mathcal{U}(t + \Delta t, t) = T \exp\left[-i\int_t^{t+\Delta t} d\tau \mathcal{H}(\tau)\right], \tag{9}$$

which is well-approximated as $\mathcal{U}(t + \Delta t, t) \approx \exp[-i\mathcal{H}(t)\Delta t]$, within numerical errors for a sufficiently short Δt. To achieve a correct wavefunction change in time, we further expand the time-evolution operator in terms of Chebishev polynomials [38, 56], which can be retrieved recursively, that is

$$\begin{aligned}\mathcal{U}(t + \Delta t; t) &= \exp\left[-i\frac{\mathcal{H}(t)}{E_0}\Delta t E_0\right] = \exp\left[-i\tilde{H}(t)\Delta\tau\right] \\ &= \sum_{k=0}^{\infty} c_k(\Delta\tau) T_k(\tilde{H}(t)),\end{aligned} \tag{10}$$

where $E_0 \equiv \max|\langle\Psi|\mathcal{H}|\Psi\rangle|$ normalizes the Hamiltonian to avoid singularities of Chebishev polynomials and

$$c_k(\Delta\tau) = \begin{cases} J_0(\Delta\tau) & (k = 0) \\ 2(-i)^k J_k(\Delta\tau) & (k \geq 1) \end{cases} \tag{11}$$

$$\begin{aligned} &T_0 = 1, \quad T_1(\tilde{H}) = \tilde{H}, \\ &T_{k+1}(\tilde{H}) = 2\tilde{H}T_k(\tilde{H}) - T_{k-1}(\tilde{H}), \end{aligned} \tag{12}$$

constitute our expansion terms. Here $\tilde{H} = \mathcal{H}/E_0$, $\Delta\tau = \Delta t E_0$, and J_k are the Bessel functions of first kind. For small $\Delta\tau$, the coefficients $c_k(\Delta\tau)$ rapidly converge to zero as k increases. Thus keeping the first few expansion terms in the right hand side of Eq.(10) is enough to reach numerically reliable results.

Figure 3 is one of the main results in this paper. In Fig.3, we illustrate how the wavefunction evolves in time in our numerical simulation of the non-Abelian braiding. We choose $|E_3\rangle$ as the initial state at $t = 0$, and take $T = 100/\Delta$. It demonstrates that only the inner part of the wave function moves in time, which exactly corresponds to the movement of Majorana mode γ_1. At $t = 6T$, although the gate configuration goes back to the initial one, the inner part of the wave function moves to the inner edge of wire 3, which indicates that γ_1 is successfully interchanged with γ_3. Then finally, the inner part goes back to the initial position at $t = t_f \equiv 12T$.

We project the same wavefunction into the instantaneous eigenstates $|\pm E_i(t)\rangle$ $(i = 1, 2, 3)$ in Fig.3 (f). Initially, the wavefunction consists of only $|E_3\rangle$, but after the gating process starts, the wave function quickly spreads over the eigenstates $|-E_3\rangle$ and $|\pm E_3\rangle$. Nevertheless, the final state ends up at $|-E_3\rangle$, as expected as the non-Abelian braiding process mentioned above.

If one operates the gates too slowly or too quickly, the non-Abelian braiding fails. For example, in the slow gating with $T = 100000/\Delta$, both inner and outer Majorana

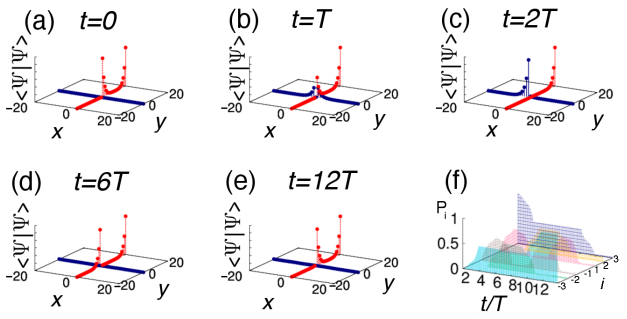

FIG. 3: (color online). γ_2 braiding with $T = 100/\Delta$. We take $\Delta = \lambda$, $\mu = 0.7\lambda$ and $N = 20$. We start with the squared wavefunction in (a) localized in wire 1, which can be seen to migrate towards the center only for γ_1 in (b). The complete transfer of γ_1 to wires 2 and 3 are respectively seen in (c) and (d). Final state at (e) indicates the return of the MBS to wire 1. (f) Projection of the wave function on the instantaneous eigenstates, $P_{\pm i}(t) = \langle\Psi(t)| \pm E_i(t)\rangle$ $(i = 1, 2, 3)$. We can observe our wavefunction begins completely on $|E_3\rangle$ and after superposing on other eigenstates, completely transfers to $|-E_3\rangle$.

modes of wire 1 move together in time, in which the state mostly stays at the instantaneous eigenstate $|E_3(t)\rangle$, as expected by the adiabatic theorem. On the other hand, for the quick gating with $T = 1/\Delta$, the wave function extends over all eigenstates $|\pm E_i(t)\rangle$ $(i = 1, 2, 3)$, and it never goes back to the initial state. In the latter case, the wave function in the final state also spreads over nanowires in space, which suggests that bulk modes are excited during the gating. We exemplify these unsuccessful braiding in Fig. 4.

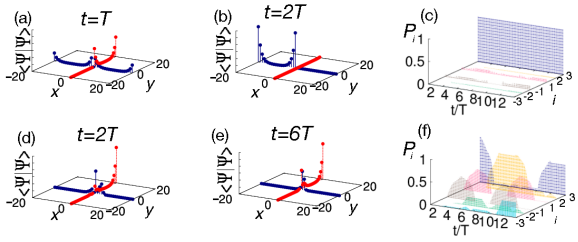

FIG. 4: (color online). Behavior outside braiding (good) conditions. (a) and (b) represent the evolution of the system on adiabatic limit ($T = 100000/\Delta$), where both Majorana edge-states migrate to the next wire, as can be seen from (b), consequently remaining on the same state, as can be observed from the projection of the wavefunction on the instantaneous eigenstates in (c). (d) and (e) account for the opposite, fast regime ($T = 1/\Delta$), with bulk excitations visible in (d) and a more erratic spread over the eigenstates in (f). We take $\Delta = \lambda$, $\mu = 0.7\lambda$, and $N = 20$.

To quantify the non-Abelian braiding, we introduce its success rate P_s as the probability that the final state

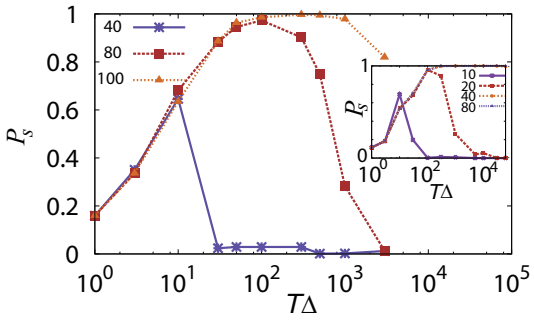

FIG. 5: (color online). Success rate P_s of the Majorana braiding. Each line accounts for a different length (in site number) of each wire (1-4), with x-axis being our operation time T, and y-axis the success rate P_s. We take $\Delta = 0.1\lambda$ and $\mu = 0.7\lambda$. The inset shows P_s for $\Delta = \lambda$. The red lines (80 and 20 sites/wire) draw a clear separation between its adiabatic (slow, large T) and dissipative (fast, small T) domains, suggesting an appreciable necessity for both size and time scale adjustment.

$|\Psi(t_f)\rangle$ is found to be the desired state $|-E_3\rangle$,

$$P_s = |\langle\Psi(t_f)| - E_3\rangle|^2 \tag{13}$$

In Fig.5, we plot the success rate P_s versus the adiabatic parameter T, with various wire lengths. The data indicates that a longer wire is desirable for the non-Abelian braiding. For longer wires, the success rate can reach the maximum, *i.e.* $P_s = 1$ for large T. In a shorter wire, on the other hand, a Majorana end mode is fairly coupled with the Majorana mode on the other end, so they tend to move together, resulting in an adiabatic process even for a moderate T. We also find that a quicker gating fails to achieve the non-Abelian braiding for any length of wires, since it excites undesirable bulk modes.

Finally, from our numerical results, we evaluate the optimal condition for non-Abelian braiding. We note that T should be larger than the inverse of the bulk gap $1/\Delta$, not to excite bulk modes. Our numerical data determines how large it should be. Figure 5 indicates that the lower bound T is not a merely $O(1/\Delta)$, but it is evaluated as $T_{\min} \sim O(10^2/\Delta)$. For a typical superconducting state with $\Delta = O(1)$ K, $T_{\min}$ can be a few nanoseconds. On the other hand, the upper bound of T can be determined as follows. As we illustrated in the above, the non-Abelian braiding is realized as an non-adiabatic process between Majorana modes. Thus, for Majorana modes with energy ϵ, ϵT should not be too large. Our numerical results imply that the success rate of the non-Abelian braiding P_s reaches almost the maximum when ϵT is less than $O(10)$. The latter condition can be easily met for long wires, since ϵ scales as $\epsilon \sim e^{-N/l_0}$. It is also found in Fig. 5 that the quantum limit of superconducting state, i.e. $\Delta/\lambda = 1$, requires less numbers of sites for the non-Abelian braiding, which is preferable if one realizes topological superconducting wires as a chain of

quantum dots.[33]

The authors are grateful to J. D. Sau and K. T. Law for fruitful discussions. This work was supported by the JSPS (No.25287085) and KAKENHI Grants-in-Aid (No.22103005) from MEXT. C.S.A. is supported by MEXT Scholarship (kokuhi-gaikokujin-ryugakusei 2013)

* Electronic address: msato@nuap.nagoya-u.ac.jp

[1] Y. Tanaka, M. Sato, and N. Nagaosa, J. Phys. Soc. Jpn. **81**, 011013 (2012).
[2] X. L. Qi and S. C. Zhang, Rev. Mod. Phys. **83**, 1057 (2011).
[3] F. Wilczek, Nat. Phys. **5**, 614 (2009).
[4] N. Read and D. Green, Phys. Rev. B **61**, 10267 (2000).
[5] D. A. Ivanov, Phys. Rev. Lett. **86**, 268 (2001).
[6] A. Y. Kitaev, Physics-Uspekhi **44**, 131 (2001).
[7] M. Sato, Phys. Rev. B **81**, 220504(R) (2010).
[8] M. Sato, Phys. Lett. B **575**, 126 (2003).
[9] L. Fu and C. L. Kane, Phys. Rev. Lett. **100**, 096407 (2008).
[10] M. Sato, Y. Takahashi, and S. Fujimoto, Phys. Rev. Lett. **103**, 020401 (2009).
[11] J. D. Sau, R. M. Lutchyn, S. Tewari, and S. D. Sarma, Phys. Rev. Lett. **104**, 040502 (2010).
[12] M. Sato and S. Fujimoto, Phys. Rev. B **79**, 094504 (2009).
[13] M. Sato, Y. Takahashi, and S. Fujimoto, Phys. Rev. B **82**, 134521 (2010).
[14] J. Alicea, Phys. Rev. B **81**, 125318 (2010).
[15] R. M. Lutchyn, J. D. Sau, and S. D. Sarma, Phys. Rev. Lett. **105**, 077001 (2010).
[16] Y. Oreg, G. Refael, and F. von Oppen, Phys. Rev. Lett. **105**, 177002 (2010).
[17] V. Mourik, K. Zuo, S. Frolov, S. Plissard, E. Bakkers, and L. Kouwenhoven, Science **336**, 1003 (2012).
[18] M. Deng, C. Yu, G. Huang, M. Larsson, P. Caro, and H. Xu, Nano Lett. **12**, 6414 (2012).
[19] A. Das, Y. Ronen, Y. Most, Y. Oreg, M. Heiblum, and H. Shtrikman, Nat. Phys. **8**, 887 (2012).
[20] J. Williams, A. Bestwick, P. Gallagher, S. Hong, Y. Cui, A. Bleich, J. Analytis, I. Fisher, and D. Goldhaber-Gordon, Phys. Rev. Lett. **109**, 056803 (2012).
[21] M. Veldhorst, M. Snelder, M. hoek, T. Gang, V. Guduru, X. L. Wang, U. Zeitler, W. G. van der Wiel, A. A. Golubov, H. Hilgenkamp, et al., Nat. Mater. **11**, 417 (2012).
[22] L. P. Rokhinson, X. Liu, and J. K. Furdyna, Nat. Phys. **8**, 795 (2012).
[23] J. Linder, Y. Tanaka, T. Yokoyama, A. Sudbo, and N. Nagaosa, Phys. Rev. Lett. **104**, 067001 (2010).
[24] M. Sato and S. Fujimoto, Phys. Rev. Lett. **105**, 217001 (2010).
[25] J. Alicea, Rep. Prog. Phys. **75**, 076501 (2012).
[26] T. D. Stanescu and S. Tewari, J. Phys.: Condens. Matter **25**, 233201 (2013).
[27] C. W. J. Beenakker, Annu. Rev. Con. Mat. Phys. **4**, 113 (2013).
[28] F. Hassler, Quantum Information Processing. Lecture notes of the 44th IFF Spring School 2013 (2013).
[29] J. D. Sau, S. Tewari, R. M. Lutchyn, T. D. Stanescu, and S. D. Sarma, Phys. Rev. B **82**, 214509 (2010).
[30] J. Klinovaja and D. Loss, Phys. Rev. B **86**, 085408 (2012).
[31] J. D. Sau, C. H. Lin, H.-Y. Hui, and S. D. Sarma, Phys. Rev. Lett. **108**, 067001 (2012).
[32] D. Chevallier, D. Sticlet, P. Simon, and C. Bena, Phys. Rev. B **87**, 165414 (2013).
[33] J. D. Sau and S. D. Sarma, Nat. Comm. **3**, 964 (2012).
[34] S. Nakosai, J. C. Budich, Y. Tanaka, B. Trauzettel, and N. Nagaosa, Phys. Rev. Lett. **110**, 117002 (2013).
[35] S. Mi, D. I. Pikulin, M. Wimmer, and C. W. J. Beenakker, Phys. Rev. B **87**, 241405 (2013).
[36] J. Alicea, Y. Oreg, G. Refael, F. von Oppen, and M. P. A. Fisher, Nat. Phys. **7**, 412 (2011).
[37] J. Sau, D. Clarke, and S. Tewari, Phys. Rev. B **84**, 094505 (2011).
[38] Q. Liang, Z. Wang, and X. Hu, Euro Physics Letters **99**, 50004 (2012).
[39] P. Kotetes, G. Schön, and A. Shnirman, Journal of the Korean Physical Society **62**, 1558 (2013).
[40] B. I. Halperin, Y. Oreg, A. Stern, G. Refael, J. Alicea, and F. von Oppen, Phys. Rev. B **85**, 144501 (2012).
[41] J. D. Sau, S. Tewari, and S. D. Sarma, Phys. Rev. A **82**, 052322 (2010).
[42] X. J. Liu, C. L. M. Wong, and K. T. Law, arXiv:1304.3765.
[43] F. Zhang, C. L. Kane, and E. J. Mele, Phys. Rev. Lett. **111**, 056403 (2013).
[44] J. Li, T. Neupert, B. A. Bernevig, and A. Yazdani, arXiv:1404.4058.
[45] L. Weithifer, P. Recher, and T. L. Schimidt, arXiv:1309.4126.
[46] T. Karzig, G. Refael, and F. von Oppen, Phys. Rev. X **3**, 041017 (2013).
[47] T. Hyart, B. van Heck, I. C. Fulga, M. Burrello, A. R. Akhmerov, and C. W. J. Beenakker, Phys. Rev. B **88**, 035121 (2013).
[48] C. V. Kraus, P. Zoller, and M. A. Baranov, Phys. Rev. Lett. **111**, 203001 (2013).
[49] X.-J. Liu and A. M. Lobos, Phys. Rev. B **87**, 060504 (2013).
[50] C.-K. Chiu, M. Vazifeh, and M. Franz, arXiv:1403.0033v1.
[51] M. Cheng, R. M. Lutchyn, V. Galitski, and S. D. Sarma, Phys. Rev. Lett. **103**, 107001 (2009).
[52] T. Mizushima and K. Machida, Phys. Rev. A **82**, 023624 (2010).
[53] M. Cheng, R. M. Lutchyn, V. Galitski, and S. D. Sarma, Phys. Rev. B **82**, 094504 (2010).
[54] M. Cheng, V. Galitski, and S. D. Sarma, Phys. Rev. B **84**, 104529 (2011).
[55] J. von Neumann and E. P. Wigner, Z. Phys. **30**, 467 (1929).
[56] H. Tal-Ezer and R. Kosloff, Jour. Chem. Phys. **81** (1984).
[57] D. Göddeke, R. Strzodka, and S. Turek, International Journal of Parallel, Emergent and Distributed Systems (IJPEDS), Special issue: Applied parallel computing **22**, 221 (2007).
[58] M. Baboulin, A. Buttari, J. Dongarra, J. Kurzak, J. Langou, J. Langou, P. Luszczek, and S. Tomov, Comp. Phys. Comm. **180**, 2526 (2009).
[59] S. L. Grand, A. W. Götz, and R. C. Walker, Comp. Phys. Comm. **184**, 374 (2013).
[60] For details, see Supplementary Material.

Supplementary Material

Calculation Method

The Hamiltonian in Eq. (1) can be recast under Bogoliubov-de Gennes representation as

$$\begin{aligned}\mathcal{H}^{\mathrm{BdG}} &= -\left[\frac{\mu}{2}+\frac{\lambda}{2}\left(\cos k_x+\cos k_y\right)\right]\tau_z \\ &\quad -\frac{\Delta}{2}e^{i\theta}\left(\sin k_x\tau_y+\sin k_y\tau_x\right), \end{aligned} \tag{1}$$

which in turn can be rewritten in real space in matrix form, defining our Hamiltonian as $H=\sum_{ij}c_i^\dagger\mathcal{H}_{\boldsymbol{i},\boldsymbol{j}}c_j$ on Nambu basis,

$$\begin{aligned}\mathcal{H}_{\boldsymbol{i},\boldsymbol{i}} &= \begin{pmatrix}-\mu & 0\\ 0 & \mu\end{pmatrix}, \\ \mathcal{H}_{\boldsymbol{i}\pm\hat{\boldsymbol{e}}_x,\boldsymbol{i}} &= \begin{pmatrix}-\lambda/2 & \mp\Delta e^{i\theta}/2\\ \pm\Delta e^{-i\theta}/2 & \lambda/2\end{pmatrix}, \\ \mathcal{H}_{\boldsymbol{i}\pm\hat{\boldsymbol{e}}_y,\boldsymbol{i}} &= \begin{pmatrix}-\lambda/2 & \mp\Delta e^{i\theta}/2\\ \mp\Delta e^{-i\theta}/2 & \lambda/2\end{pmatrix}, \end{aligned} \tag{2}$$

where $\boldsymbol{i}$ represents site position, assuming lattice constant to be 1. To numerically evaluate our system, we take each wire length to be n sites long with one central site linking them. Each gate is represented as a factor $g_i\in[0,1]$ $(i=1,2,3,4)$ multiplying the Hamiltonian elements between the central site and its neighbors in real space,

$$\begin{aligned}\mathcal{H}_{\hat{\boldsymbol{e}}_y,0} &= g_1\begin{pmatrix}-\lambda/2 & -ie^{i\theta}\Delta/2\\ -ie^{-i\theta}\Delta/2 & \lambda/2\end{pmatrix}, \\ \mathcal{H}_{-\hat{\boldsymbol{e}}_x,0} &= g_2\begin{pmatrix}-\lambda/2 & e^{i\theta}\Delta/2\\ -e^{-i\theta}\Delta/2 & \lambda/2\end{pmatrix}, \\ \mathcal{H}_{-\hat{\boldsymbol{e}}_y,0} &= g_3\begin{pmatrix}-\lambda/2 & ie^{-i\theta}\Delta/2\\ ie^{-i\theta}\Delta/2 & \lambda/2\end{pmatrix}, \\ \mathcal{H}_{\hat{\boldsymbol{e}}_x,0} &= g_4\begin{pmatrix}-\lambda/2 & -e^{i\theta}\Delta/2\\ e^{-i\theta}\Delta/2 & \lambda/2\end{pmatrix}. \end{aligned} \tag{3}$$

For a linear gate operation in the interval of time T as described in this work, a gate being turned on (off) is taken to evolve as $g_i=t/T$ $(g_i=1-t/T)$, counting the time t from the beginning of the operation. More general functions may be used for operating both gates smoothly at the same time. Finally, to achieve the wavefunction change in time, we expand the time-evolution operator in terms of Chebishev polynomials[56], which can be retrieved recursively, that is

$$\begin{aligned}\mathcal{U}(t+\Delta t;t) &= \exp\left[-i\frac{\mathcal{H}(t)}{E_0}\Delta t E_0\right]=\exp\left[-i\tilde{H}(t)\Delta\tau\right] \\ &= \sum_{k=0}^{\infty}c_k(\Delta\tau)T_k(\tilde{H}(t)), \end{aligned} \tag{4}$$

$E_0\equiv\max|\langle\Psi|\mathcal{H}|\Psi\rangle|$ normalizes the Hamiltonian to avoid singularities and

$$c_k(\Delta\tau)=\begin{cases}J_0(\Delta\tau) & (k=0)\\ 2(-i)^kJ_k(\Delta\tau) & (k\geq 1)\end{cases} \tag{5}$$

$$\begin{aligned}&T_0=1,\quad T_1(\tilde{H})=\tilde{H},\\ &T_{k+1}(\tilde{H})=2\tilde{H}T_k(\tilde{H})-T_{k-1}(\tilde{H}),\end{aligned} \tag{6}$$

constitute our expansion terms. J_k are the Bessel functions of first kind, and their value is used to choose truncation point under double precision. While one can apply the above operator successively, obtaining the desired wavefunction in time t, this process is needlessly slow if done completely in double precision. Mixed precision[57–59] can be efficiently applied for a boost in calculation speed if instead of calculating the wavefunction, only its variation is evaluated. Explicitly, this can be illustrated on the following steps:

$$\begin{aligned}&\Psi(t+\Delta t)_{\mathrm{dl}}=\mathcal{U}(t+\Delta t;t)\Psi(t)_{\mathrm{dl}}\\ &\rightarrow\Delta\Psi_{\mathrm{dl}}=(\mathcal{U}(t+\Delta t;t)-1)\Psi(t)_{\mathrm{dl}}\end{aligned} \tag{7}$$

$$\begin{aligned}\Delta\Psi &=_{\mathrm{dl}}\left(\sum_{k=0}^{k'}c_kT_k(\tilde{H})-1\right)_{\mathrm{fl}}\Psi(t)_{\mathrm{fl}}\\ &=_{\mathrm{dl}}\left[(c_0-1)_{\mathrm{fl}}+\sum_{k=1}^{k'}c_{k,\mathrm{fl}}T_k(\tilde{H})_{\mathrm{fl}}\right]\Psi(t)_{\mathrm{fl}}\\ \Psi(t+\Delta t) &=_{\mathrm{dl}}\Psi(t)_{\mathrm{dl}}+\Delta\Psi_{\mathrm{dl}}\end{aligned} \tag{8}$$

Here the subscript dl (fl) represents a double (single) precision conversion/variable. For example, equation 7 represents a common time-evolution process done with double precision variables. The following expression claims a conversion of $\Psi(t)$ from double to single precision, as well as a single precision expansion of the time-evolution operator, while $=_{\mathrm{dl}}$ implies that these data should be converted to double precision when adding to build up $\Delta\Psi$. Similarly, on the following line we point that the zero-order term should be changed to single precision after calculating it in double precision, and each other expansion term is calculated with single precision T_k and c_k. Shortly, each term in our expansion is calculated as a vector in single precision, being later added as a double precision variation to the double precision wavefunction. Note that the wavefunction is converted to single precision for time evolution, but computed as double precision in the end of each step. In fact, we start our evaluation with an eigenstate of the Hamiltonian taken in double precision, and only its variation, which corresponds to most of the computations, is found in single precision steps.

It is important to note that this method relies on the constraint of small dt to work, as well as small and smooth wavefunction variation, otherwise single precision computation of the expansion terms may cumulate a

large error. Nevertheless, this constraint is also required for the very numeric expansion of the time-evolution operator, in order to ignore its intrinsic time-ordering operator to a good approximation. In other words, the possibility to evaluate time-evolution of the wavefunction in real space-time already gives us the possibility of a mixed precision method. Concretely, in our case each $\Delta\Psi \sim 10^{-7}$, which in single precision allows for good enough numeric results in the $10^{-7} \sim 10^{-14}$ range, which accounts for first order terms, as well as $10^{-9} \sim 10^{-16}$ for the next order, all of them well fit in the limit of double precision, up to 10^{-15}. Therefore, summing these terms up on double precision avoids greater errors from ignoring their contribution, which forcedly would happen if they were added completely in single precision.